Progress In Electromagnetics Research B, Vol. 77, 85–101, 2017

Semi-Analytical Modeling of Spoke-Type Permanent-Magnet Machines Considering the Iron Core Relative Permeability: Subdomain Technique and Taylor Polynomial

Lazhar Roubache[1, *], Kamel Boughrara[1], Frédéric Dubas[2], and Rachid Ibtiouen[1]

Abstract—This article presents a novel contribution to the improvement of the analytic modeling of electrical machines using two-dimensional (2-D) subdomain technique with Taylor polynomial. To validate this novel method, the semi-analytical model has been implemented for spoke-type permanent-magnet (PM) machines (STPMM). Magnetostatic Maxwell's equations are solved in polar coordinates and in all parts of the machine. The global solution is obtained by using the traditional boundary conditions (BCs), in addition to new radial BCs (e.g., between the PMs and the rotor teeth) which are traduced into a system of linear equations according to Taylor series expansion. The magnetic field calculations are performed for two different values of iron core relative permeability (viz., 10 and 1,000) and compared to finite-element method (FEM) predictions. The results show that a very good agreement is obtained.

1. INTRODUCTION

The full calculation of magnetic field in electrical machines is the first step for their design and optimization. The methods of magnetic field prediction can be classified in various categories [1]: Lehmann's graphical, numerical equivalent circuit, Schwarz-Christoffel mapping, Maxwell-Fourier Some comprehensive reviews of magnetic field prediction in electrical machine can be found in [1–8], and their references. Numerical methods (i.e., the finite-element, finite-difference, or boundary-element analysis) [9–11], which can be classified as the very accurate method compared to the real results with large flexibility to various geometries, include nonlinear and nonhomogeneous materials. The most accurate models are three-dimensional (3-D) numerical methods. However, these approaches are very time-consuming and not very suitable for optimization analysis. Nevertheless, in [12, 13], it is possible to optimize electromagnetic systems from numerical methods. Nowadays, in order to reduce the computation time, hybrid numerical methods can be developed [14]. The actual design works are mainly based on (semi-)analytical models (i.e., equivalent circuit, SC mapping and Maxwell-Fourier methods) [1]. These approaches have been proposed under some geometrical and physical assumptions. Maxwell-Fourier methods are one of the most resent semi-analytic approaches with good accurate results in 2D or 3-D electromagnetic performance calculation. These models are based on the formal resolution of Maxwell's equations applied in each subdomain of the electromagnetic devices. These subdomains can be divided into two types of subdomains, viz., periodic (e.g., air-gap) and non-periodic (e.g., slots, teeth, tooth-tips...). In the second type, the general solution is derived by applying homogeneous Neumann BCs. These conditions are obtained from the approximation that the iron parts are considered to be infinitely permeable. In the literature, we find the applications of these methods for the analysis of

Received 10 May 2017, Accepted 8 July 2017, Scheduled 27 July 2017
* Corresponding author: Lazhar Roubache (roubache.lazhar@gmail.com).
[1] Ecole Nationale Polytechnique (LRE-ENP), Algiers, 10, Av. Pasteur, El Harrach, BP 182, 16200, Algeria. [2] Département ENERGIE, FEMTO-ST, CNRS, Univ. Bourgogne Franche-Comté, Belfort, France.

several types of electrical machines, such as [2, 7, 8, 15–19] for PM synchronous machines, [20–22] for solid or cage rotor induction motors, and [23–25] for reluctance machines. It is interesting to note that an overview on the existing (semi-)analytical models in Maxwell-Fourier methods with the local/global saturation has been realized in [1], whose some details and the (dis)advantages of these techniques can be found. In [6, 23–25], the authors approximate the adjacent regions (e.g., rotor slots/teeth)in the harmonic modeling technique as one homogeneous region with a relative permeability developed as a Fourier series expansion. In [1], Dubas and Boughrara developed the first model introducing the iron parts in the magnetic field calculation using subdomain technique, where the authors solved partial differential equations (EDPs) of magnetic potential vector in Cartesian coordinates in which the subdomains connection is performed directly in both directions (i.e., x- and y-edges). However, to apply this contribution in the modulation of electrical machines, it should transform it to polar coordinates. Thus, the work in this paper takes part in the development and improvement of the subdomain technique on the scientific topic.

The aim of this paper is to propose a new contribution improving 2-D subdomain technique with Taylor polynomial by focusing on the consideration of iron. The proposed technique involves solution in polar coordinates of Laplace's and Poisson's equations in the stator yoke, stator slots and teeth, air-gap, rotor teeth, PMs, and rotor nonmagnetic regions. For the rotor (i.e., PMs/teeth) and stator (i.e., slots/teeth), we take the general solution considering the nonhomogeneous Neumann BCs. In addition to traditional interface conditions between two adjacent regions represented with radius value and interval of angles (e.g., between the air-gap and stator slots/teeth), we add the consideration of the interface conditions between two adjacent regions represented with angle value and interval of radius (e.g., between the PMs and the rotor teeth). The first type of interface conditions permits to get a system of linear equations according to Fourier series expansion, and the second type permits to obtain a system of equations according to Taylor series expansion. All results from the developed semi-analytical model are then compared to those found by FEM [26].

2. PROBLEM DEFINITIONS

2.0.1. Magnetic Field Solution

Figure 1 represents the topology of fractional-slot STPM machines with the definition of region where Region I represents the air-gap, Region II the nonmagnetic material under rotor magnetic (i.e., under PMs and rotor teeth), Region III the stator yoke, Region IV the buried PMs, Region V the rotor

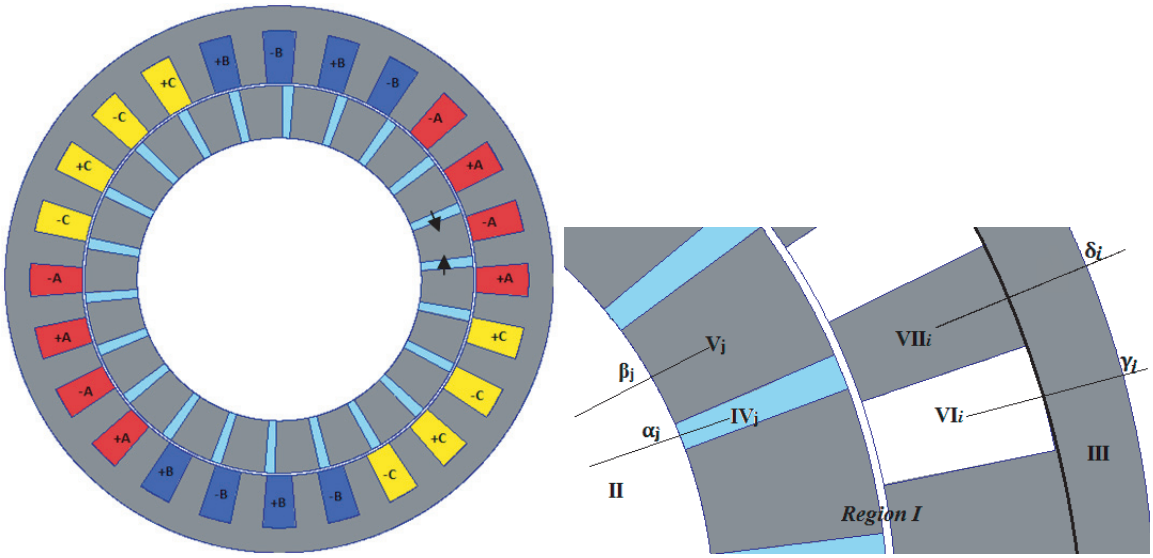

Figure 1. Example of fractional-slot STPM machines (i.e., 24-slots/22-poles) with the definition of regions.

teeth, Region VI the stator slots, and Region VII the stator teeth. The 2-D semi-analytical model is formulated in magnetic vector potential A_z and polar coordinates (r, θ) with the following assumptions:

- the end-effects are neglected (i.e., that the magnetic variables are independent of z);
- the stator tooth-tips and rotor bridge are not considered. However, they can be introduced easily;
- the stator slots/teeth, rotor teeth and PMs have radial sides;
- the current density has only one component along the z-axis;
- the electrical conductivities of materials are assumed to be null (i.e., the eddy-currents induced in the copper/iron/PMs are neglected);
- the PMs demagnetization curve is assumed to be linear;
- the direction of PMs magnetization is supposed purely tangential, i.e., $\overrightarrow{M} = \{0, M_\theta, 0\}$

In this article, we take into account the iron core relative permeability in stator (i.e., yoke and teeth) and rotor (i.e., teeth) subdomain regions.

The general EDP issued from magnetostatic Maxwell's equations in a continuous and isotopic region can be expressed, in term of magnetic potential vector A_z, by

$$\Delta A_z(r,\theta) = 0, \quad \text{in Region I, II, III, V, and VII} \tag{1}$$

$$\Delta A_z(r,\theta) = -\mu_0 \nabla \times \overrightarrow{M}, \quad \text{in Region IV} \tag{2}$$

$$\Delta A_z(r,\theta) = -\mu_0 J_z, \quad \text{in Region VI} \tag{3}$$

where $\overrightarrow{M}$ is the PMs magnetization, J_z the current density in the stator slots, and μ_0 the vacuum permeability. The field vectors $\overrightarrow{B} = \{B_r;\ B_\theta;\ 0\}$ and $\overrightarrow{H} = \{H_r;\ H_\theta;\ 0\}$ in the different regions are coupled by:

$$\overrightarrow{B} = \mu_0 \overrightarrow{H}, \quad \text{in Region I, II, and VI} \tag{4}$$

$$\overrightarrow{B} = \mu_0 \mu_{rm} \overrightarrow{H} + \mu_0 \overrightarrow{M}, \quad \text{in Region IV} \tag{5}$$

$$\overrightarrow{B} = \mu_0 \mu_{rc} \overrightarrow{H}, \quad \text{in Region III, V, and VII} \tag{6}$$

where μ_{rm} is the relative recoil permeability of PMs, and μ_{rc} is the relative permeability of the iron core. Using $\overrightarrow{B} = \nabla \times \overrightarrow{A}$, the r- and θ-components of magnetic flux density are deduced from A_z by

$$B_r = \frac{1}{r}\frac{\partial A}{\partial \theta} \quad \text{and} \quad B_\theta = -\frac{\partial A}{\partial r} \tag{7}$$

2.1. General Solution of Laplace's Equation with Nonhomogeneous Neumann BCs

In a general case of electrical machine analysis using subdomain technique, the iron parts are considered to have infinite relative permeability (which leads to homogeneous Neumann BCs in slots/PMs/teeth subdomains), and Laplace's, Poisson's or Helmholtz's equations should be solved only in slots/PMs/Air-gap regions [8, 20]. In order to add rotor/stator teeth in the magnetic field prediction in electrical machines, it is necessary to consider the general solution of Maxwell's equations with nonhomogeneous Neumann BCs.

In slots/PMs/teeth subdomains, we have to solve the Laplace's equation in polar coordinates

$$\frac{\partial^2 A_z(r,\theta)}{\partial r^2} + \frac{1}{r}\frac{\partial A_z(r,\theta)}{\partial r} + \frac{1}{r^2}\frac{\partial^2 A_z(r,\theta)}{\partial \theta^2} = 0 \tag{8}$$

The electrical machines have cylindrical form, and the following periodicity condition between 0 and 2π should be added to solution

$$A_z(r,\theta)|_{\theta=0} = A_z(r,\theta)|_{\theta=2\pi} \tag{9}$$

Considering the periodicity condition given in Eq. (9), the general solution of Eq. (8) can be written as

$$A_z(r,\theta) = D1_0 + D2_0 \ln(r) + \sum_{k=1}^{\infty}\left(D1_k r^k + D2_k r^{-k}\right)\sin(k\,(\theta-\theta_1)) + \sum_{k=1}^{\infty}\left(D3_k r^k + D4_k r^{-k}\right)\cos(k\,(\theta-\theta_1)) \tag{10}$$

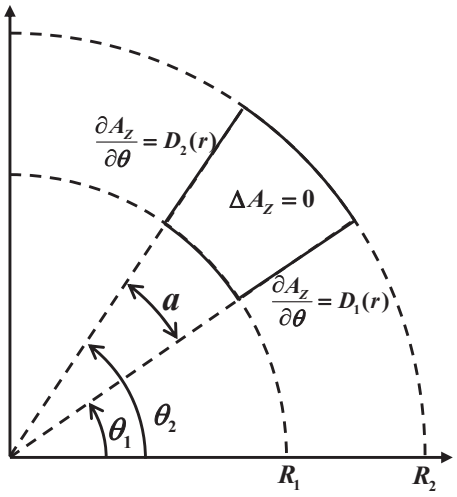

Figure 2. Slots/PMs/teeth subdomains with nonhomogeneous Neumann BCs.

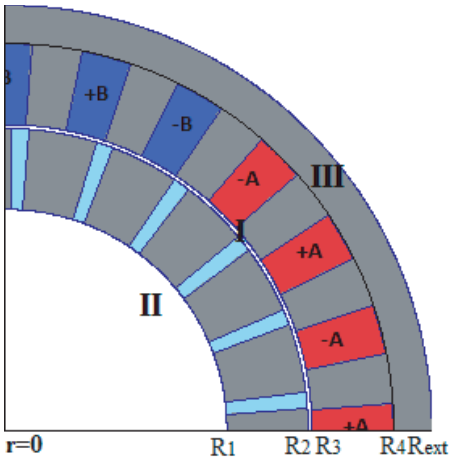

Figure 3. Description: Air-gap (i.e., Region I), nonmagnetic material under rotor magnetic (i.e., Region II) and stator yoke (Region III).

where k is a positive integer, and $D1_0 - D4_k$ are the integration constants.

As shown in Figure 2, the slots/PMs/teeth subdomains are delimited by $r \in [R_1;\ R_2] \wedge \theta \in [\theta_1;\ \theta_2]$ and are associated with the following BCs:

$$D_1(r) = \left.\frac{\partial A(r,\theta)}{\partial \theta}\right|_{\theta=\theta_1} = \sum_{k=1}^{\infty} k\left(D1_k r^k + D2_k r^{-k}\right) \tag{11a}$$

$$D_2(r) = \left.\frac{\partial A(r,\theta)}{\partial \theta}\right|_{\theta=\theta_2} = \sum_{k=1}^{\infty} k\left(D1_k r^k + D2_k r^{-k}\right)\cos(ka) + \sum_{k=1}^{\infty} k\left(D3_k r^k + D4_k r^{-k}\right)\sin(ka) \tag{11b}$$

In the case where $D_1(r) = D_2(r) = 0$ (i.e., homogeneous Neumann BCs), the derivation of Eqs. (11a) and (11b) gives

$$\sum_{k=1}^{\infty} k\left(D1_k r^k + D2_k r^{-k}\right) = 0 \quad \Rightarrow \quad D1_k = D2_k = 0 \tag{12a}$$

$$\sum_{k=1}^{\infty} k\left(D3_k r^k + D4_k r^{-k}\right)\sin(k\,a) = 0 \quad \Rightarrow \quad k = \frac{m\pi}{a} \tag{12b}$$

where m is a positive integer, and the solution of Eq. (10) can be simplified as

$$A_z(r,\theta) = D1_0 + D2_0 \ln(r) + \sum_{m=1}^{\infty}\left(D3_m r^{\frac{m\pi}{a}} + D4_m r^{-\frac{m\pi}{a}}\right)\cos\left(\frac{m\pi}{a}(\theta - \theta_1)\right) \tag{13}$$

As explicated in [1], $D1_0 - D4_m$ can be determined by Fourier series expansions associated with BCs for the radii R_1 and R_2. In the general case where the variation of A_z versus θ for $\theta = \theta_1$ and $\theta = \theta_2$ is not necessarily null, it should consider the general solution of Eq. (10), which can be written with another form as

$$\begin{aligned} A_z = {} & D1_0 + D2_0 \ln(r) + \sum_{m=1}^{\infty}\left(B1_m r^{\frac{m\pi}{a}} + B2_m r^{-\frac{m\pi}{a}}\right)\cos\left(\frac{m\pi}{a}(\theta - \theta_1)\right) \\ & + \sum_{k=1}^{\infty}\left(D1_k r^k + D2_k r^{-k}\right)\sin(k(\theta - \theta_1)) + \sum_{\substack{k=1 \\ k\neq\frac{m\pi}{a}}}^{\infty}\left(D3_k r^k + D4_k r^{-k}\right)\cos(k(\theta - \theta_1)) \end{aligned} \tag{14}$$

where $B1_m$ & $B2_m$ are new integration constants which respectively represent $D3_k$ & $D4_k$ for $k = m\pi/a$. It is interesting to note that the added Fourier constants $D1_k - D4_k$ can be determined by Taylor series expansions associated with BCs for θ_1 and θ_2, and some explanations of the obtained equations are explained in Section 2.6. The solution of Poisson's equations is derived by adding the corresponding particular solution.

2.2. Solution of Laplace's Equation in Regions I, II and III

1) Air-gap (Region I): In the air-gap, which is an annular domain at $r \in [R_2;\ R_3]$ (see Figure 3), the solution of Eq. (1) is defined by

$$A_{zI}(r,\theta) = A1_0 + A2_0 \ln(r) + \sum_{n=1}^{\infty} \left(A1_n r^n + A2_n r^{-n}\right) \sin(n\theta) + \sum_{n=1}^{\infty} \left(A3_n r^n + A4_n r^{-n}\right) \cos(n\theta) \quad (15)$$

where n is a positive integer, and $A1_0 - A4_n$ are the integration constants in Region I.

2) Nonmagnetic Material under Rotor Magnetic (Region II): The general solution in this subdomain has the same form as the solution in Region I. Nevertheless, in adding the condition of the finite value of A_z for $r = 0$, the solution can be written as

$$A_{zII}(r,\theta) = \sum_{n=1}^{\infty} A5_n r^n \sin(n\theta) + \sum_{n=1}^{\infty} A6_n r^n \cos(n\theta) \quad (16)$$

where $A5_n$ & $A6_n$ are the integration constants in Region II.

3) Stator Yoke (Region III): In the stator yoke, which is an annular domain at $r \in [R_4;\ R_{ext}]$ (see Figure 3), the general solution has the same form as the solution in Region I. Nevertheless, in adding the Dirichlet's BC for $r = R_{ext}$, the solution can be written as

$$A_{zIII}(r,\theta) = \sum_{n=1}^{\infty} A7_n \left(\left(\frac{r}{R_{ext}}\right)^n - \left(\frac{r}{R_{ext}}\right)^{-n}\right) \sin(n\theta) + \sum_{n=1}^{\infty} A8_n \left(\left(\frac{r}{R_{ext}}\right)^n - \left(\frac{r}{R_{ext}}\right)^{-n}\right) \cos(n\theta) \quad (17)$$

where $A7_0 - A8_n$ are the integration constants in Region III.

2.3. Solution of Poisson's Equation with Nonhomogeneous Neumann in Regions IV and VI

1) Buried PMs (Region IV): In each buried PM subdomain (j) of Region IV (see Figure 1), we have to solve Eq. (2), i.e., Poisson's equation. Because the direction of PMs Magnetization is purely tangential, Eq. (2) can be reduced to

$$\frac{\partial^2 A_z(r,\theta)}{\partial r^2} + \frac{1}{r}\frac{\partial A_z(r,\theta)}{\partial r} + \frac{1}{r^2}\frac{\partial^2 A_z(r,\theta)}{\partial \theta^2} = -\mu_0 \frac{M_\theta}{r} \quad (18)$$

where $M_\theta = M_j = (-1)^j \cdot B_{rm}/\mu_0$ with j varying from 1 to $2p$ poles, and B_{rm} is the remanent flux density of PMs.

As shown in Figure 4(a), the jth PM is associated with nonhomogeneous Neumann BCs, and using the method explicated in Section 2.2, the solution of Eq. (18) can be written as

$$\begin{aligned} A_{zIVj}(r,\theta) \ = \ & B1_{j0} + B2_{j0} \ln(r) - \mu_0 M_j r + \sum_{m=1}^{\infty} \left(B1_{jm} r^{\frac{m\pi}{a}} + B2_{jm} r^{-\frac{m\pi}{a}}\right) \cos\left(\frac{m\pi}{a}\left(\theta - \alpha_j + \frac{a}{2}\right)\right) \\ & + \sum_{k=1}^{\infty} \left(D1_{jk} r^k + D2_{jk} r^{-k}\right) \sin\left(k\left(\theta - \alpha_j + \frac{a}{2}\right)\right) \\ & + \sum_{\substack{k=1 \\ k \neq \frac{m\pi}{a}}}^{\infty} \left(D3_{jk} r^k + D4_{jk} r^{-k}\right) \cos\left(k\left(\theta - \alpha_j + \frac{a}{2}\right)\right) \end{aligned} \quad (19)$$

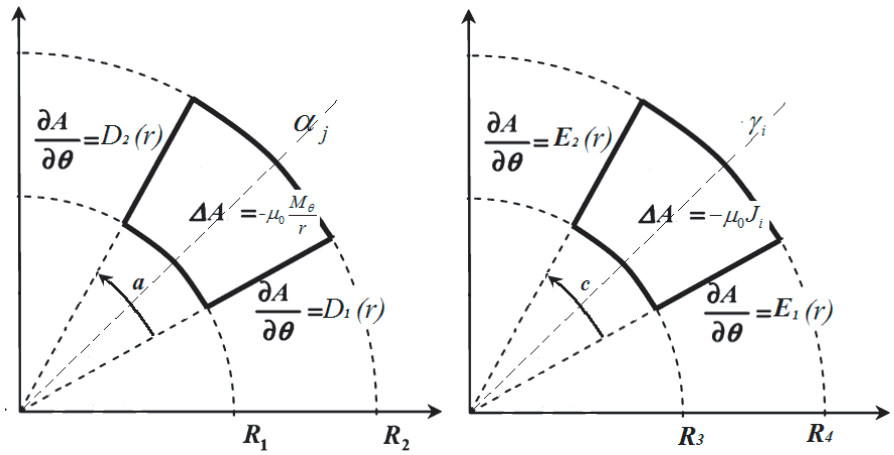

Figure 4. Nonhomogeneous Neumann BCs for (a) jth buried PMs and (b) ith stator slot.

where m and k are the positive integers; $B1_{j0} - B2_{jm}$ and $D1_{jk} - D4_{jk}$ are the integration constants; α_j is the angular position of the jth PMs; a is the PM-opening.

*2) Stator Slots (Region VI):*In each slot subdomain (i) of Region VI, we have to solve Eq. (2), i.e., Poisson's equation,

$$\frac{\partial^2 A_z(r,\theta)}{\partial r^2} + \frac{1}{r}\frac{\partial A_z(r,\theta)}{\partial r} + \frac{1}{r^2}\frac{\partial^2 A_z(r,\theta)}{\partial \theta^2} = -\mu_0 J_i \tag{20}$$

where J_{zi} is the current density in the ith stator slot with i varying from 1 to Q_s in which Q_s represents the number of stator slots.

Taking into account the BCs shown in Figure 4(b), the solution of Eq. (20) can be written as

$$A_{zVIi}(r,\theta) = C1_{i0} + C2_{i0}\ln(r) - \frac{1}{4}\mu_0 J_i r^2 + \sum_{m=1}^{\infty}\left(C1_{im}r^{\frac{m\pi}{c}} + C2_{im}r^{-\frac{m\pi}{c}}\right)\cos\left(\frac{m\pi}{c}\left(\theta - \gamma_i + \frac{c}{2}\right)\right)$$
$$+\sum_{k=1}^{\infty}\left(E1_{ik}r^{k} + E2_{ik}r^{-k}\right)\sin\left(k\left(\theta - \gamma_i + \frac{c}{2}\right)\right) + \sum_{\substack{k=1\\k\neq\frac{m\pi}{c}}}^{\infty}\left(E3_{ik}r^{k} + E4_{ik}r^{-k}\right)\cos\left(k\left(\theta - \gamma_i + \frac{c}{2}\right)\right) \tag{21}$$

where m and k are the positive integers; $C1_{i0} - C2_{im}$ and $E1_{ik} - E4_{ik}$ are the integration constants; γ_i is the angular position of the ith stator slot; c is the stator slot-opening.

2.3.1. Solution of Laplace's Equation with Nonhomogeneous Neumann BCs in Regions V and VII

1) Rotor Teeth (Region V): The jth rotor tooth is a subdomain region with nonhomogeneous Neumann BCs as shown in Figure 5(a). As explicated in Section 2.2, the solution of Eq. (1), i.e., Laplace's equation, can be written as

$$\begin{aligned} A_{zVj}(r,\theta) \;=\; & B3_{j0} + B4_{j0}\ln(r) + \sum_{l=1}^{\infty}\left(B3_{jl}r^{\frac{l\pi}{b}} + B4_{jl}r^{-\frac{l\pi}{b}}\right)\cos\left(\frac{l\pi}{b}\left(\theta - \beta_j + \frac{b}{2}\right)\right) \\ & + \sum_{k=1}^{\infty}\left(D5_{jk}r^{k} + D6_{jk}r^{-k}\right)sin\left(k\left(\theta - \beta_j + \frac{b}{2}\right)\right) \\ & + \sum_{\substack{k=1\\k\neq\frac{l\pi}{b}}}^{\infty}\left(D7_{jk}r^{k} + D8_{jk}r^{-k}\right)\cos\left(k\left(\theta - \beta_j + \frac{b}{2}\right)\right) \end{aligned} \tag{22}$$

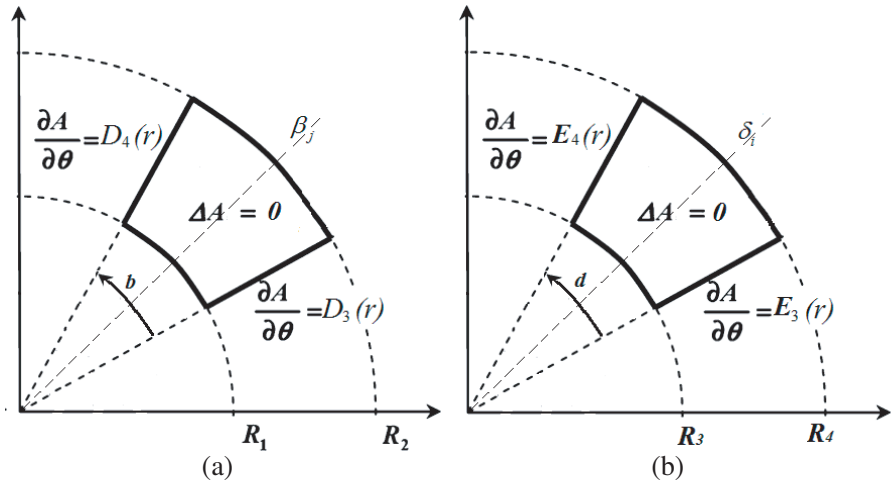

Figure 5. Nonhomogeneous Neumann BCs for (a) jth rotor and (b) ith stator teeth.

where l and k are the positive integers; $B3_{j0} - B4_{jl}$ and $D5_{jk} - D8_{jk}$ are the integration constants; β_j is the angular position of the j^{th} rotor teeth; b is the rotor tooth-opening.

2) Stator Teeth (Region VII): The ith stator tooth is a subdomain region with nonhomogeneous Neumann BCs shown in Figure 5(b). As explained in Section 2.2, the solution of Eq. (1), i.e., Laplace's equation, can be written as

$$\begin{aligned} A_{zVIIi}(r,\theta) \;=\; & C3_{i0} + C4_{i0}\ln(r) + \sum_{l=1}^{\infty}\left(C3_{il}r^{\frac{l\pi}{d}} + C4_{il}r^{-\frac{l\pi}{d}}\right)\cos\left(\frac{l\pi}{d}\left(\theta - \delta_i + \frac{d}{2}\right)\right) \\ & + \sum_{k=1}^{\infty}\left(E5_{ik}r^{k} + E6_{ik}r^{-k}\right)\sin\left(k\left(\theta - \delta_i + \frac{d}{2}\right)\right) \\ & + \sum_{\substack{k=1 \\ k\neq\frac{l\pi}{d}}}^{\infty}\left(E7_{ik}r^{k} + E8_{ik}r^{-k}\right)\cos\left(k\left(\theta - \delta_i + \frac{d}{2}\right)\right) \end{aligned} \tag{23}$$

where l and k are the positive integers; $C3_{i0} - C4_{il}$ and $E5_{ik} - E8_{ik}$ are the integration constants; δ_i is the angular position of the ith stator teeth; d is the stator tooth-opening.

2.3.2. Interfaces Conditions between Regions

To determine the integration constants in Eqs. (15)–(17), (19), and (21)–(23), the BCs at the interface between the various regions should be introduced.

The interfaces conditions in this model can be divided into two types. One is over angle interval for given radius value $\{R_1,\ R_2,\ R_3,\ R_4\}$, and the other is over radius interval for given angle $\{\alpha_j \pm a/2,\ \beta_j \pm b/2,\ \gamma_i \pm c/2,\ \delta_i \pm d/2\}$. As the obtained equations from each type of these interfaces conditions have the same form, it is sufficient to show one example for each type. The interface conditions are:

- between Region IV, V and I at $r = R_2$:

$$A_{zI}(R_2,\theta) \;=\; A_{zIVj}(R_2,\theta) \quad \text{for} \quad \alpha_j - \frac{a}{2} \le \theta \le \alpha_j + \frac{a}{2} \tag{24}$$

$$A_{zI}(R_2,\theta) \;=\; A_{zVj}(R_2,\theta) \quad \text{for} \quad \beta_j - \frac{b}{2} \le \theta \le \beta_j + \frac{b}{2} \tag{25}$$

$$H_{\theta I}(R_2,\theta) \;=\; H_{\theta IVj}(R_2,\theta) \quad \text{for} \quad \alpha_j - \frac{a}{2} \le \theta \le \alpha_j + \frac{a}{2} \tag{26}$$

$$H_{\theta I}(R_2,\theta) = H_{\theta Vj}(R_2,\theta) \quad \text{for} \quad \beta_j - \frac{b}{2} \le \theta \le \beta_j + \frac{b}{2} \tag{27}$$

- between Region IV and V at $\alpha_j + a/2 = \beta_j - b/2$ and $\alpha_{j+1} - a/2 = \beta_j + b/2$ for $r \in [R_1;\ R_2]$:

$$A_{zIVj}\left(r, \alpha_j + \frac{a}{2}\right) = A_{zVj}\left(r, \beta_j - \frac{b}{2}\right) \tag{28}$$

$$H_{r\,IVj}\left(r, \alpha_j + \frac{a}{2}\right) = H_{r\,Vj}\left(r, \beta_j - \frac{b}{2}\right) \tag{29}$$

$$A_{zIV(j+1)}\left(r, \alpha_{j+1} - \frac{a}{2}\right) = A_{zVj}\left(r, \beta_j + \frac{b}{2}\right) \tag{30}$$

$$H_{r\,IV(j+1)}\left(r, \alpha_{j+1} - \frac{a}{2}\right) = H_{r\,Vj}\left(r, \beta_j + \frac{b}{2}\right) \tag{31}$$

The interface conditions in Eqs. (24)–(27) concern regions with different subdomain frequencies which need Fourier series expansions to satisfy equalities of magnetic potential vector and tangential magnetic field. According to Fourier series expansion, the interface condition in Eq. (24) gives

$$\begin{aligned}
&B1_{j0} + B2_{j0}\ln(R_2) - \mu_0 M_j R_2 + \frac{1}{a}\sum_{k=1}^{\infty}\left(D1_{jk}R_2^{k} + D2_{jk}R_2^{-k}\right)\int_{\alpha_j-\frac{a}{2}}^{\alpha_j+\frac{a}{2}}\sin\left(k\left(\theta-\alpha_j+\frac{a}{2}\right)\right)d\theta \\
&+\frac{1}{a}\sum_{\substack{k=1\\k\neq\frac{m\pi}{a}}}^{\infty}\left(D3_{jk}R_2^{k} + D4_{jk}R_2^{-k}\right)\int_{\alpha_j-\frac{a}{2}}^{\alpha_j+\frac{a}{2}}\cos\left(k\left(\theta-\alpha_j+\frac{a}{2}\right)\right)d\theta = \frac{1}{a}\int_{\alpha_j-\frac{a}{2}}^{\alpha_j+\frac{a}{2}} A_I(R_2,\theta)d\theta
\end{aligned} \tag{32}$$

$$\begin{aligned}
&B1_{jm}R_2^{\frac{m\pi}{a}} + B2_{jm}R_2^{-\frac{m\pi}{a}} + \frac{2}{a}\sum_{k=1}^{\infty}\left(D1_{jk}R_2^{k} + D2_{jk}R_2^{-k}\right)\int_{\alpha_j-\frac{a}{2}}^{\alpha_j+\frac{a}{2}}\sin\left(k\left(\theta-\alpha_j+\frac{a}{2}\right)\right)\cos\left(\frac{m\pi}{a}\left(\theta-\alpha_j+\frac{a}{2}\right)\right)d\theta \\
&+\frac{2}{a}\sum_{\substack{k=1\\k\neq\frac{m\pi}{a}}}^{\infty}\left(D3_{jk}R_2^{k} + D4_{jk}R_2^{-k}\right)\int_{\alpha_j-\frac{a}{2}}^{\alpha_j+\frac{a}{2}}\cos\left(k\left(\theta-\alpha_j+\frac{a}{2}\right)\right)\cos\left(\frac{m\pi}{a}\left(\theta-\alpha_j+\frac{a}{2}\right)\right)d\theta \\
&= \frac{2}{a}\int_{\alpha_j-\frac{a}{2}}^{\alpha_j+\frac{a}{2}} A_I(R_2,\theta)\cos\left(\frac{m\pi}{a}\left(\theta-\alpha_j+\frac{a}{2}\right)\right)d\theta
\end{aligned} \tag{33}$$

The interface condition in Eq. (25) gives

$$\begin{aligned}
&B3_{j0} + B4_{j0}\ln(R_2) + \frac{1}{a}\sum_{k=1}^{\infty}\left(D5_{jk}R_2^{k} + D6_{jk}R_2^{-k}\right)\int_{\beta_j-\frac{b}{2}}^{\beta_j+\frac{b}{2}}\sin\left(k\left(\theta-\beta_j+\frac{b}{2}\right)\right)d\theta \\
&+\frac{1}{b}\sum_{\substack{k=1\\k\neq\frac{m\pi}{a}}}^{\infty}\left(D7_{jk}R_2^{k} + D8_{jk}R_2^{-k}\right)\int_{\beta_j-\frac{b}{2}}^{\beta_j+\frac{b}{2}}cos\left(k\left(\theta-\beta_j+\frac{b}{2}\right)\right)d\theta = \frac{1}{b}\int_{\beta_j-\frac{b}{2}}^{\beta_j+\frac{b}{2}} A_I(R_2,\theta)d\theta
\end{aligned} \tag{34}$$

$$B3_{jm}R_2^{\frac{m\pi}{a}} + B4_{jm}R_2^{-\frac{m\pi}{a}} + \frac{2}{b}\sum_{k=1}^{\infty}\left(D5_{jk}R_2^{k} + D6_{jk}R_2^{-k}\right)\int_{\beta_j+\frac{b}{2}}^{\beta_j+\frac{b}{2}}\sin\left(k\left(\theta-\beta_j+\frac{b}{2}\right)\right)\cos\left(\frac{m\pi}{a}\left(\theta-\beta_j+\frac{b}{2}\right)\right)d\theta$$

$$+\frac{2}{b}\sum_{\substack{k=1\\k\neq\frac{m\pi}{b}}}^{\infty}\left(D7_{jk}R_2^k+D8_{jk}R_2^{-k}\right)\int_{\beta_j+\frac{b}{2}}^{\beta_j+\frac{b}{2}}\cos\left(k\left(\theta-\beta_j+\frac{b}{2}\right)\right)\cos\left(\frac{m\pi}{a}\left(\theta-\beta_j+\frac{b}{2}\right)\right)d\theta$$

$$=\frac{2}{b}\int_{\beta_j+\frac{b}{2}}^{\beta_j+\frac{b}{2}}A_I(R_2,\theta)\cos\left(\frac{m\pi}{a}\left(\theta-\beta_j+\frac{b}{2}\right)\right)d\theta \tag{35}$$

The interfaces conditions in Eqs. (26) and (27) give

$$\frac{A2_0}{R_2}=\frac{1}{2\pi}\sum_{j=1}^{Q_r}\int_{\alpha_j-\frac{a}{2}}^{\alpha_j+\frac{a}{2}}H_{\theta IVj}(R_2,\theta)d\theta+\frac{1}{2\pi}\sum_{j=1}^{Q_r}\int_{\beta_j-\frac{b}{2}}^{\beta_j+\frac{b}{2}}H_{\theta Vj}(R_2,\theta)d\theta \tag{36}$$

$$\frac{-n}{\mu_0}\left(A1_nR_2^{n-1}-A2_nR_2^{-n-1}\right)=\frac{1}{\pi}\sum_{j=1}^{Q_r}\int_{\alpha_j-\frac{a}{2}}^{\alpha_j+\frac{a}{2}}H_{\theta IVj}(R_2,\theta)\sin(n\theta)d\theta+\frac{1}{\pi}\sum_{j=1}^{Q_r}\int_{\beta_j-\frac{b}{2}}^{\beta_j+\frac{b}{2}}H_{\theta Vj}(R_2,\theta)\sin(n\theta)d\theta \tag{37}$$

$$\frac{-n}{\mu_0}\left(A3_nR_2^{n-1}-A4_nR_2^{-n-1}\right)=\frac{1}{\pi}\sum_{j=1}^{Q_r}\int_{\alpha_j-\frac{a}{2}}^{\alpha_j+\frac{a}{2}}H_{\theta IVj}(R_2,\theta)\cos(n\theta)d\theta+\frac{1}{2\pi}\sum_{j=1}^{Q_r}\int_{\beta_j-\frac{b}{2}}^{\beta_j+\frac{b}{2}}H_{\theta Vj}(R_2,\theta)\cos(n\theta)d\theta \tag{38}$$

The interface conditions in Eqs. (28)–(31) concern two polynomials equations with a different degree, which need Taylor series expansions around R_t such as $R_t\in]R_1;\ R_2]$ to satisfy equalities of magnetic potential vector and radial magnetic field. The Taylor polynomial degree is chosen to satisfy the lack of equations obtained by Fourier series expansion of previous interface conditions compared to the number of unknowns in system, so for k varying from 1 to K_r it is enough to take Taylor polynomial of degree $2K_r-1$. Therefore, the interface condition in Eq. (28) gives

$$A_{IVj}\left(R_t,\alpha_j+\frac{a}{2}\right)=A_{Vj}\left(R_t,\beta_j-\frac{b}{2}\right) \tag{39}$$

$$\frac{\partial^k A_{IVj}}{\partial r^k}\left(R_t,\alpha_j+\frac{a}{2}\right)=\frac{\partial^k A_{Vj}}{\partial r^k}\left(R_t,\beta_j-\frac{b}{2}\right) \tag{40}$$

From the interface condition in Eq. (29), we get

$$Hr_{IVj}\left(R_t,\alpha_j+\frac{a}{2}\right)=Hr_{Vj}\left(R_t,\beta_j-\frac{b}{2}\right) \tag{41}$$

$$\frac{\partial^k Hr_{IVj}}{\partial r^k}\left(R_t,\alpha_j+\frac{a}{2}\right)=\frac{\partial^k Hr_{Vj}}{\partial r^k}\left(R_t,\beta_j-\frac{b}{2}\right) \tag{42}$$

From the interface condition in Eq. (30), we get

$$A_{IVj+1}\left(R_t,\alpha_{j+1}-\frac{a}{2}\right)=A_{Vj}\left(R_t,\beta_j+\frac{b}{2}\right) \tag{43}$$

$$\frac{\partial^k A_{IVj+1}}{\partial r^k}\left(R_t,\alpha_j+\frac{a}{2}\right)=\frac{\partial^k A_{Vj}}{\partial r^k}\left(R_t,\beta_j-\frac{b}{2}\right) \tag{44}$$

From the interface condition in Eq. (31), we get

$$Hr_{IVj+1}\left(R_t,\alpha_{j+1}-\frac{a}{2}\right)=Hr_{Vj}\left(R_t,\beta_j+\frac{b}{2}\right) \tag{45}$$

$$\frac{\partial^k Hr_{IVj+1}}{\partial r^k}\left(R_t,\alpha_j+\frac{a}{2}\right)=\frac{\partial^k Hr_{Vj}}{\partial r^k}\left(R_t,\beta_j-\frac{b}{2}\right) \tag{46}$$

There are no simple expressions to define the system obtained by Taylor series expansions (39)–(46). However, the coefficients of the unknowns in this system can be defined recursively. For example, the development of interface conditions (Eq. (39)) and (Eq. (40)) permits to define new coefficients C_{B1k} for the vector potential of region IV as

$$\begin{cases} k=0 & B1_{j0}+\ldots+B1_{jm}R_t^{\frac{m\pi}{a}}\cos(m\pi)+\ldots=A_{zVj}\left(R_t,\beta_j-\dfrac{b}{2}\right) & \Rightarrow & C_{B1\,0}=R_t^{\frac{m\pi}{a}}\cos(m\pi) \\ k=1 & \dfrac{B2_{j0}}{R_t}+\ldots+B1_{jm}\dfrac{m\pi}{a\,R_t}R_t^{\frac{m\pi}{a}}\cos(m\pi)+\ldots=\dfrac{\partial A_{zVj}}{\partial r}\left(R_t,\beta_j-\dfrac{b}{2}\right) & & C_{B1\,1}=\dfrac{m\pi}{a\,R_t}C_{B1\,0} \\ k=2 & \dfrac{-B2_{j0}}{R_t^2}+\ldots+B1_{jm}\dfrac{m\pi}{a\,R_t}\dfrac{\frac{m\pi}{a}-1}{R_t}R_t^{\frac{m\pi}{a}}\cos(m\pi)+\ldots=\dfrac{\partial^2 A_{zVj}}{\partial r^2}\left(R_t,\beta_j-\dfrac{b}{2}\right) & & C_{B1\,2}=\dfrac{\frac{m\pi}{a}-1}{R_t}C_{B1\,1} \end{cases} \tag{47}$$

The coefficients $C_{B1\,k}$ can be defined by the recursive formula as:

$$\begin{cases} C_{B1\,0}=R_t^{\frac{m\pi}{a}}\cos(m\pi) \\ C_{B1\,k+1}=\frac{\frac{m\pi}{a}+1-k}{R_t}C_{B1\,k} \end{cases} \tag{48}$$

The other coefficients are deduced with the same reasoning.

It is interesting to note that the interface conditions for the radii $\{R_1,\ R_3,\ R_4\}$ and for the angels $\{\gamma_i \pm c/2,\ \delta_i \pm d/2\}$ are developed with the same previous method

3. RESULTS AND VALIDATION

The developed semi-analytical method for fractional-slot STPM machines taking into account the iron core relative permeability is used to determine electromagnetic performances (viz., the magnetic flux density, the magnetic flux linkage, the back EMF, the electromagnetic/cogging/ripple torques, the non-intrinsic unbalanced magnetic forces,...) whose various formulas have been clarified in [19].

The main dimensions and parameters of the fractional-slot STPM machines (e.g., 24-slots/22-poles) with the buried PMs and a single layer winding are given in Table 1. Then, semi-analytic results are verified by 2-D FEM [26]. For the finite-elements simulation, we have used 99,199 nodes and 194,796 elements.

Table 1. Parameters of the studied machine.

Symbol	Parameters	Value (Units)
B_{rm}	Remanence flux density of PMs	1.2 (T)
μ_{rm}	Relative permeability of PMs	1
N_c	Number of conductors per stator slot	108
I_m	Peak phase current	18 (A)
Q_s	Number of stator slots	24
c	Stator slot-opening	7.5 (deg)
a	PM-opening	3.27 (deg)
p	Number of pole pairs	11
R_{ext}	Radius of the external stator surface	110 (mm)
R_4	Outer radius of stator slot	100 (mm)
R_3	Radius of the stator outer surface	79 (mm)
R_2	Radius of the rotor inner surface at the PM surface	78 (mm)
R_1	Radius of the rotor inner surface at the PM bottom	57 (mm)
g	Air-gap length	1 (mm)
L_u	Axial length of the machine	63 (mm)
Ω	Mechanical pulse of synchronism	1,100 (rpm)

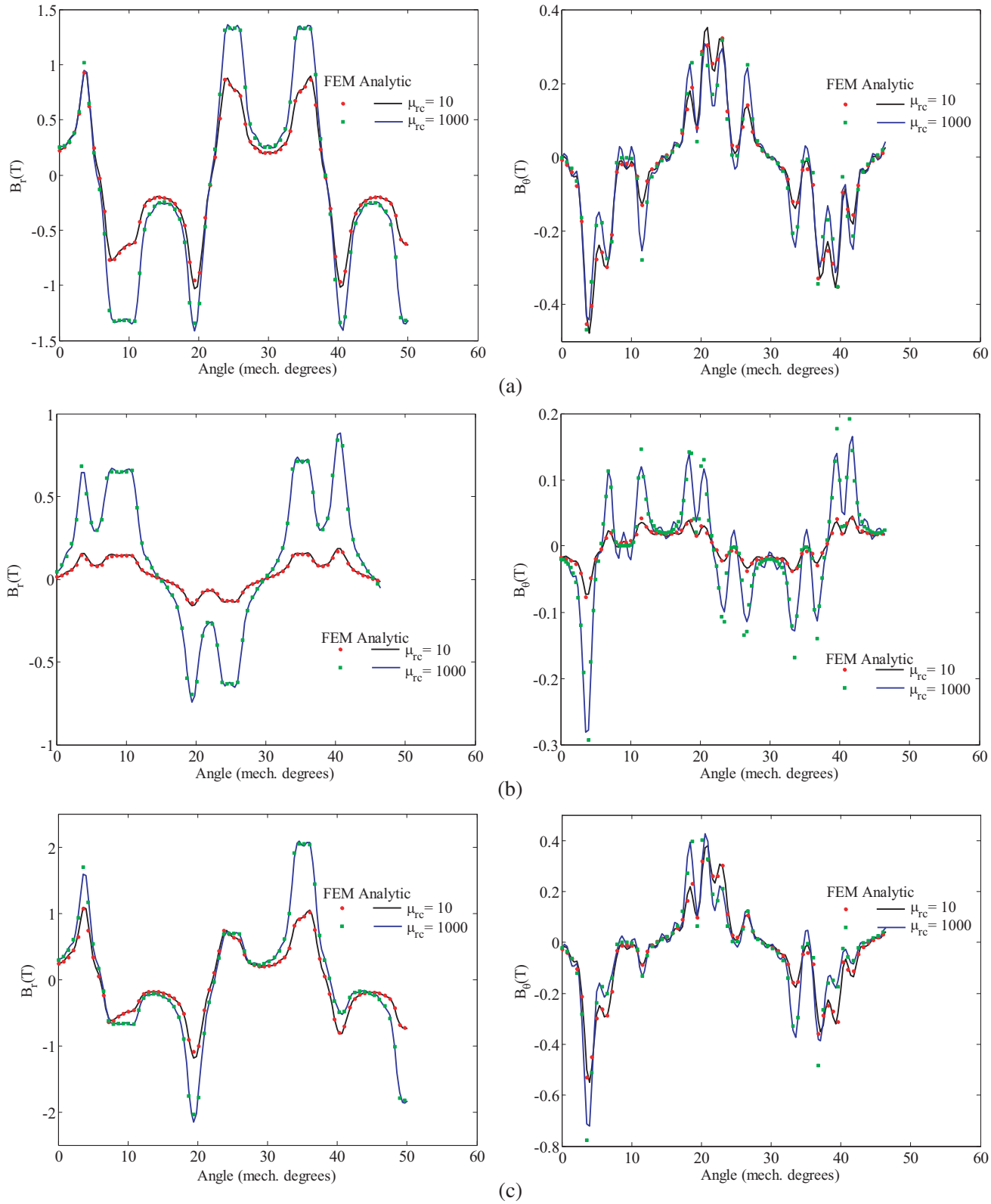

Figure 6. Radial and tangential components of the magnetic flux density in the middle of the air-gap (i.e., Region I): (a) PMs alone, (b) stator current alone and (c) on load condition.

The waveforms of radial and tangential components of the magnetic flux density in the various regions are computed with a finite number of harmonic terms, viz., $N = 200$, $M = L = 20$ and $K = 2$. The analytic calculation of magnetic flux distribution in all regions is done with two different values of the iron core relative permeability (viz., 10 and 1,000). In each case, the relative permeability is supposed the same for all iron parts (i.e., stator yoke, stator and rotor teeth). However, it should be noted that it is possible to take special permeability value for each region.

In Figure 6, a comparison between the numerical results and semi-analytical predictions is shown in term of the magnetic flux density in the middle of the air-gap (i.e., Region I) for three operating conditions : i) PMs alone, ii) stator currents alone, and iii) on load condition. One can see that the diminution of the iron core relative permeability is accompanied by a decrease in magnetic flux amplitude. It can be seen that a very good agreement for the radial and tangential components of the magnetic flux density is obtained.

The proposed model is characterized by the ability to know the magnetic flux density in all machine regions, such as stator/rotor yoke, stator slots, stator/rotor teeth and PMs. Figure 7(a) shows the radial and tangential components of the magnetic flux density in the middle of the PMs/rotor teeth under a pole-pitch for on load condition. Very good agreement is obtained for the tangential component. For

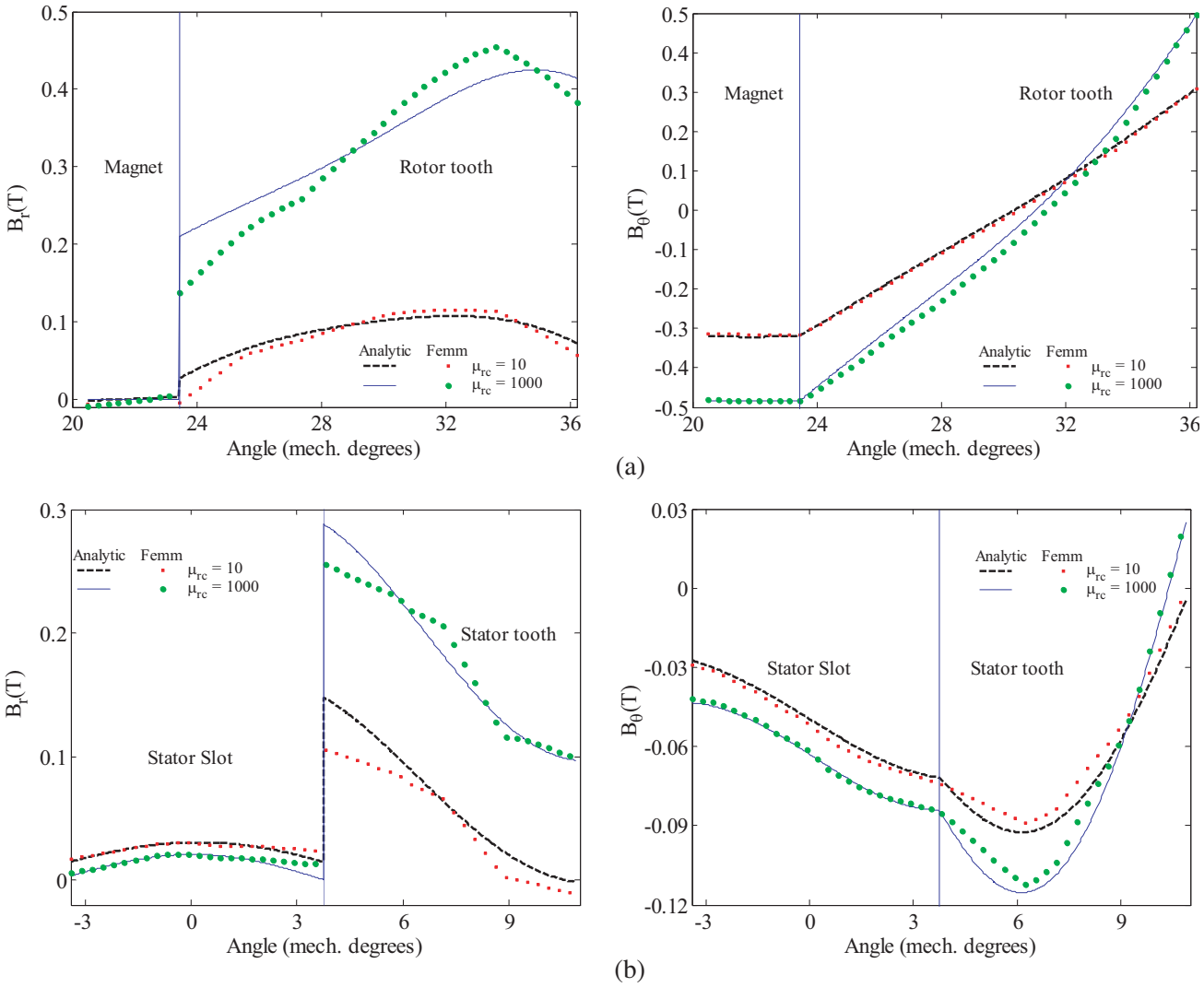

Figure 7. Radial and tangential components of the magnetic flux density under tooth-pitch for on load condition in the middle of (a) PMs/rotor tooth and (b) stator slot/tooth.

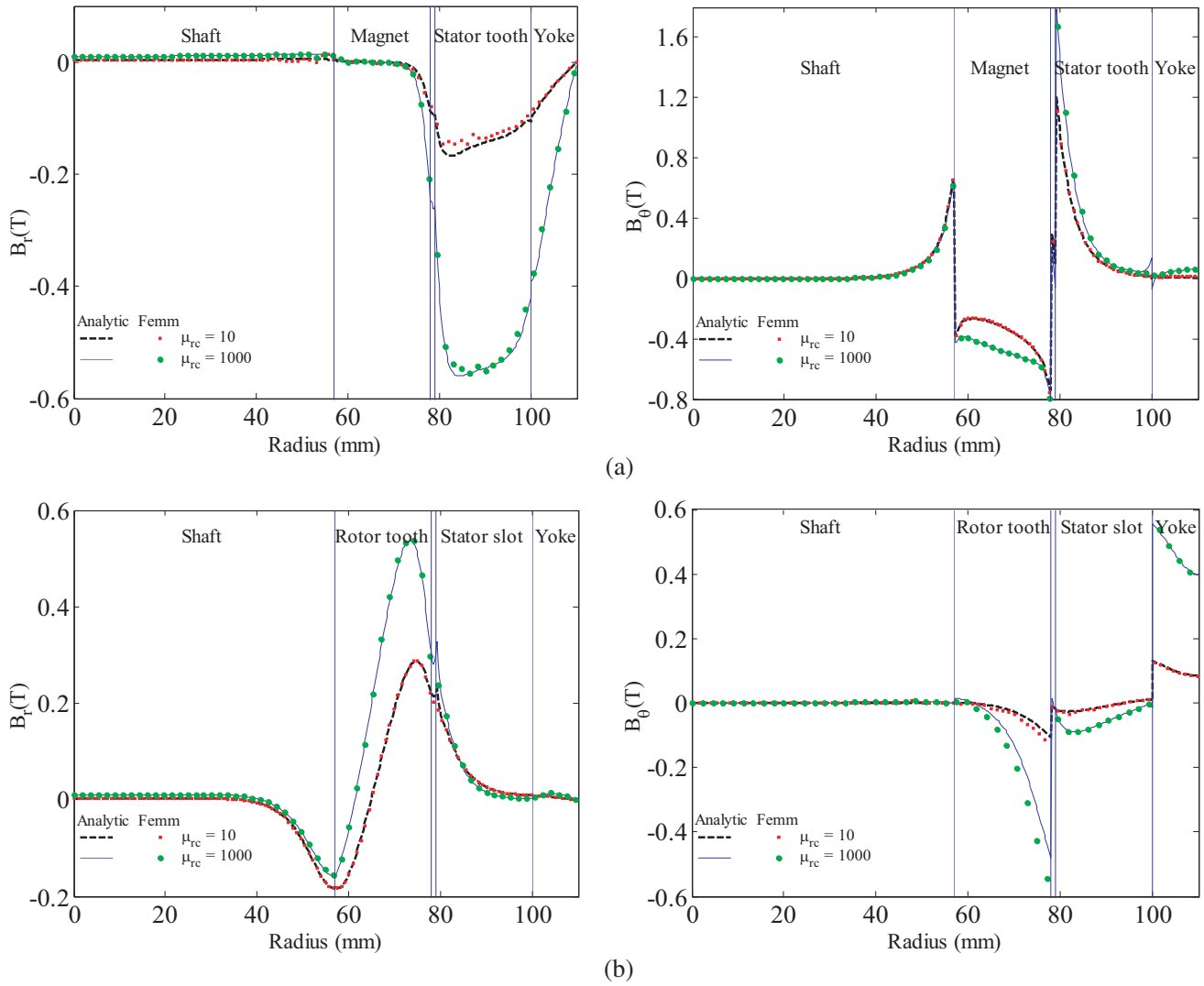

Figure 8. Radial and tangential components of the magnetic flux density for on load condition at: (a) $\theta = \alpha_1$ and (b) $\theta = \gamma_3$.

the radial component, the results are good with agreeable error, the same order of accuracy is seen for stator slot/teeth under a tooth-pitch shown in Figure 7(b).

Another presentation of obtaining results is shown in Figure 8, where the radial and tangential components of the magnetic flux density for on load condition are plotted in function of the radius at a given angle. For the semi-analytic results, the magnetic flux density is calculated for each interval of radius by the corresponding solution. The results are obtained for $\theta = \alpha_1$ and $\theta = \gamma_3$, and very good agreement is obtained.

The static torque versus rotor position is presented in Figure 9(a). The stator currents are supposed constant, and the rotor position is updated to have nominal rotation speed. As obtained, the mechanical angle has $\Theta_{rs} = 2\pi/p$ fundamental period, and the maximum torque is obtained for $\Theta_{rs} = \pi/2p$. The maximum torque decreases for small value of relative permeability. It can be seen that a very good agreement is obtained for the two proposed values of relative permeability. Figure 9(b) shows the electromagnetic torque waveform versus electrical angle. At each instant, the stator currents are updated to have a sinusoidal current waveform. The initial rotor position is taken for giving maximum torque value, i.e., $\Theta_{rs0} = \pi/2p$.

The induced back EMF for no-load condition is shown in Figure 10. The simulation is done for

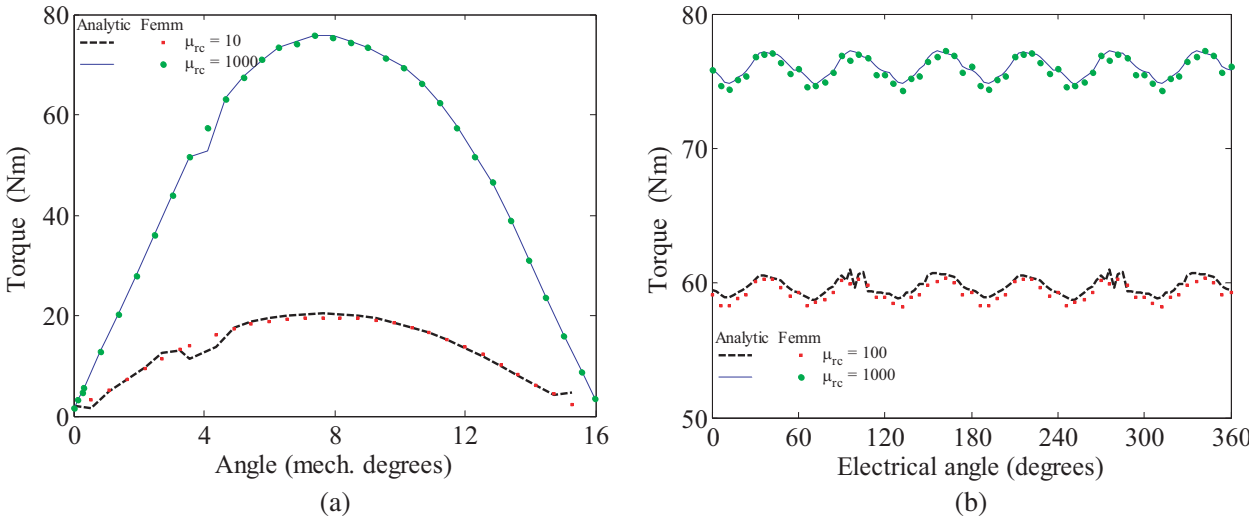

Figure 9. (a) Static torque and (b) electromagnetic torque at $\Theta_{rs0} = \pi/2p$ for on load condition (with $I = 18\,\mathrm{A}$).

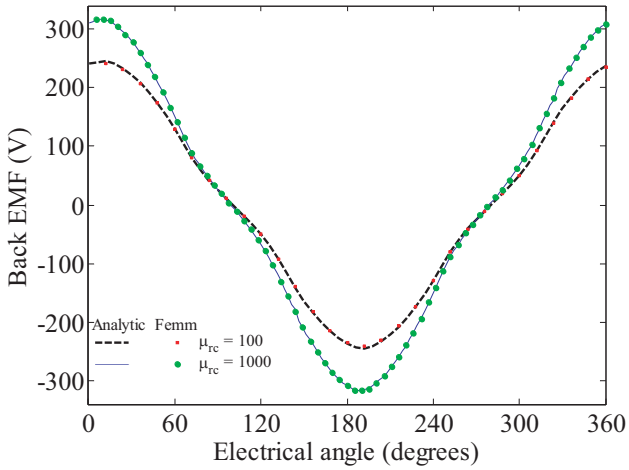

Figure 10. Induced back EMF for no-load condition (with $I = 0\,\mathrm{A}$).

two different values of iron core relative permeability, and the obtained results confirm the accuracy of the proposed semi-analytical model.

Figure 11(a) shows the evolution of simulation time versus the number of harmonics. To reduce the computation time of the semi-analytical model, the number of spatial harmonics N, M, L and K can be reduced. However, this leads to reduction in accuracy. It is seen that for a giving value of spatial harmonics, the RMS error will not be affected very much by increasing the number of spatial harmonics. This value can be chosen as an optimal value. Figure 11(b) shows the evolution of RMS error for the radial component of the magnetic flux density in the middle of the air-gap versus harmonic order of Regions I, II, and III (i.e., N) for several values of harmonic order of the other regions. The RMS error is calculated by

$$error = \sqrt{\sum_{m=1}^{N_{pc}} \left(B_{Ir,m}^{Numeric} - B_{Ir,m}^{Analytic}\right)^2 \Big/ N_{pc}} \tag{49}$$

It can be seen from Figure 11(b) that the error starts to converge around $N = 180$, $M = L = 6$ and $K = 1$.

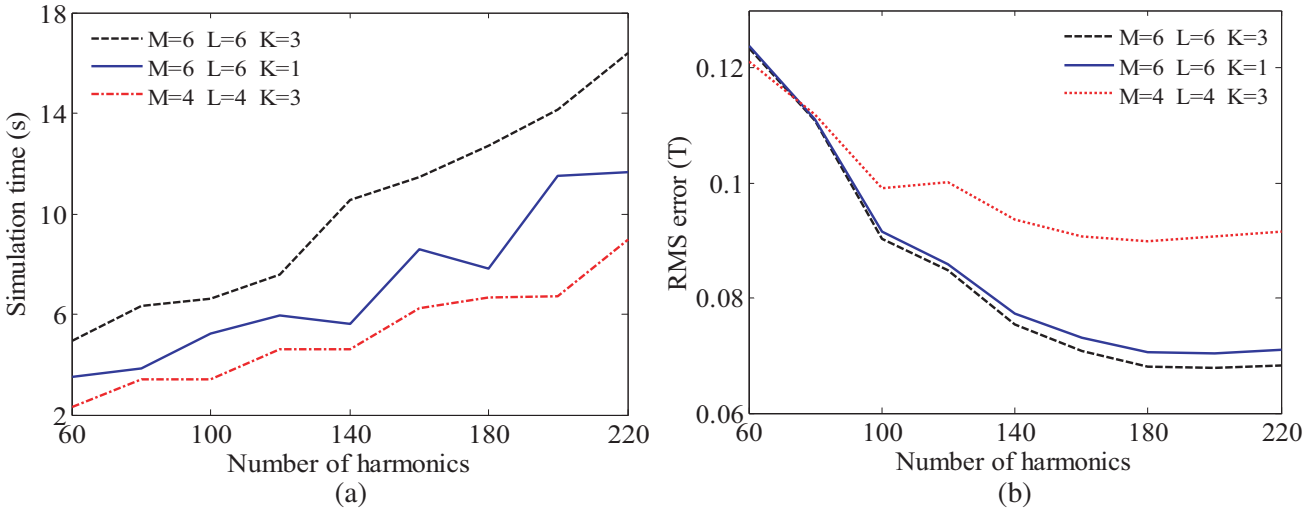

Figure 11. Influence of the number of harmonics associated with Regions I, II and III (i.e., N) on the radial component of the magnetic flux density in the middle of the air-gap versus numeric simulations for several values of the number of harmonics associated with the other regions: (a) the calculation time and (b) the RMS error.

4. CONCLUSION

In this paper, we have proposed an improved semi-analytical model based on subdomain technique with Taylor polynomial for prediction open-circuit, armature reaction and on load magnetic field distribution in STPM machines. The proposed model takes into account the relative permeability in all machine regions including the iron parts.

One of the largest advantages of the discussed approach is its ability to account the finite permeability in rotor/stator teeth and yoke, with the possibility to get the solution of magnetic flux in these regions. Currently, only linear PM material proprieties are considered. However, nonlinear PM materials could be accounted by means of an iterative algorithm, and also the proposed model offers the possibility to take especial finite permeability for each PM or rotor/stator teeth, same for rotor and stator yoke.

Semi-analytic results are in excellent agreement with the ones obtained by 2-DFEM. From these results, we show the accuracy of the semi-analytical model for several values of iron core relative permeability.

APPENDIX A. NOMENCLATURE

$H_{rx}, H_{\theta x}$ Radial and tangential components of the magnetic flux intensity in x domain where x can be I, II, III, IV, V, VI, or VII.

$A_{z\,x}$ Magnetic potential vector in x domain.

α_j, a Position and opening width of j^{th} PMs.

β_j, b Position and opening width of j^{th} rotor tooth.

γ_i, c Position and opening width of i^{th} stator slot.

δ_i, d Position and opening width of i^{th} stator tooth.

n Harmonic order for air-gap, nonmagnetic material, and stator yoke.

k, m, l Harmonic order for slots/PMs/teeth.

J_z Current density.

μ_0 Vacuum permeability.

μ_{rc} Relative permeability of iron core.

μ_{rm} Relative permeability of PMs.

REFERENCES

1. Dubas, F. and K. Boughrara, "New scientific contribution on the 2-D subdomain technique in cartesian coordinates: Taking into account of iron parts," *Math. Comput. Appl.*, Vol. 22, No. 1, 17, 2017, DOI: 10.3390/mca22010017.
2. Dubas, F. and C. Espanet, "Analytical solution of the magnetic field in permanent-magnet motors taking into account slotting effect: no-load vector potential and flux density calculation," *IEEE Trans. on Magn.*, Vol. 45, No. 5, 2097–2109, 2009.
3. Devillers, E., J. Le Besnerais, T. Lubin, M. Hecquet, and J. P. Lecointe, "A review of subdomain modeling techniques in electrical machines: Performances and applications," *Proc. ICEM*, Lausanne, Switzerland, Sep. 4–7, 2016.
4. Tiegna, H., Y. Amara, and G. Barakat, "Overview of analytical models of permanent magnet electrical machines for analysis and design purposes," *Mathematics and Computer in Simulation*, Vol. 90, 162–177, 2013.
5. Curti, M., J. J. H. Paulides, and E. A. Lomonova, "An overview of analytical methods for magnetic field computation," *Proc. EVER*, Grimaldi Forum, Monaco, Mar. 31–Apr. 02, 2015.
6. Sprangers, R. L. J., J. J. H. Paulides, B. L. J. Gysen, and E. A. Lomonova, "Magnetic saturation in semi-analytical harmonic modeling for electric machine analysis," *IEEE Trans. on Magn.*, Vol. 52, No. 2, Art. ID 8100410, 2016.
7. Pfister, P.-D., X. Yin, and Y. Fang, "Slotted permanent-magnet machines: General analytical model of magnetic fields, torque, eddy currents, and permanent-magnet power losses including the Diffusion effect," *IEEE Trans. on Magn.*, Vol. 52, No. 5, Art. ID 8103013, 2016.
8. Dubas, F. and A. Rahideh, "Two-dimensional analytical permanent-magnet eddy-current loss calculations in slotless PMSM equipped with surface-inset magnets," *IEEE Trans. on Magn.*, Vol. 50, No. 3, Art. ID 6300320, 2014.
9. Yilmaz, M. and P. T. Krein, "Capabilities of finite element analysis and magnetic equivalent circuits for electrical machine analysis and design," *Proc. PESC*, Rhodes, Greece, Jun. 15–19, 2008.
10. Sulaiman, E. B., F. Khan, and T. Kosaka, "Field-excited flux switching motor design, optimization and analysis for future hybrid electric vehicle using finite element analysis," *Progress In Electromagnetics Research B*, Vol. 71, 153–166, 2016.
11. Konwar, R. S., K. Kalita, A. Banerjee, and W. K. S. Khoo, "Electromagnetic analysis of a bridge configured winding cage induction machine using finite element method," *Progress In Electromagnetics Research B*, Vol. 48, 347–373, 2013.
12. Schutte, J. and J. M. Strauss, "Optimization of a transverse flux linear PM generator using 3D finite element analysis," *Proc. ICEM*, Rome, Italy, Sep. 6–8, 2010.
13. Espanet, C., C. Kieffer, A. Mira, S. Giurgea, and F. Gustin, "Optimal design of a special permanent magnet synchronous machine for magnetocaloric refrigeration," *Proc. ECCE*, Denver, CO, USA, Sep. 15–19, 2013.
14. Benlamine, R., F. Dubas, S.-A. Randi, D. Lhotellier, and C. Espanet, "3-D numerical hybrid method for PM eddy-current losses calculation: Application to axial-flux PMSMs," *IEEE Trans. on Magn.*, Vol. 51, No. 7, Art. ID 8106110, 2015.
15. Rahideh, A., H. Moayed-Jahromi, M. Mardaneh, F. Dubas, and T. Korakianitis, "Analytical calculations of electromagnetic quantities for slotted Brushless machines with surface-inset magnets," *Progress In Electromagnetics Research B*, Vol. 72, 49–65, 2017.
16. Teymoori, S., A. Rahideh, H. Moayed-Jahromi, and M. Mardaneh, "2-D analytical magnetic field prediction for consequent-pole permanent magnet synchronous machines," *IEEE Trans. on Magn.*, Vol. 52, No. 6, Art. ID 8202114, 2016.
17. Boughrara, K., T. Lubin, R. Ibtiouen, and N. Benallal, "Analytical calculation of parallel double excitation and spoke-type permanent-magnet motors; simplified versus exact model," *Progress In Electromagnetics Research B*, Vol. 47, 145–178, 2013.
18. Lubin, T., S. Mezani, and A. Rezzoug, "Two-dimensional analytical calculation of magnetic field and electromagnetic torque for surface-inset permanent-magnet motors," *IEEE Trans. on Magn.*,

Vol. 48, No. 6, 2080–2091, 2012.

19. Boughrara, K., R. Ibtiouen, and F. Dubas, "Analytical prediction of electromagnetic performances and unbalanced magnetic forces in fractional-slot spoke-type permanent-magnet machines," *Proc. ICEM*, Lausanne, Switzerland, Sep. 4–7, 2016.
20. Boughrara, K., N. Takorabet, R. Ibtiouen, O. Touhami, and F. Dubas, "Analytical analysis of cage rotor induction motors in healthy, defective, and broken bars conditions," *IEEE Trans. on Magn.*, Vol. 51, No. 2, Art. ID 8200317, 2015.
21. Roubache, L., K. Boughrara, and R. Ibtiouen, "Analytical electromagnetic analysis of multi-phases cage rotor induction motors in healthy, broken bars and open phases conditions," *Progress In Electromagnetics Research B*, Vol. 70, 113–130, 2016.
22. Boughrara, K., F. Dubas, and R. Ibtiouen, "2-D analytical prediction of eddy currents, circuit model parameters, and steady-state performances in solid rotor induction motors," *IEEE Trans. on Magn.*, Vol. 50, No. 12, Art. ID 7028214, 2014.
23. Sprangers, R. L. J., J. J. H. Paulides, B. L. J. Gysen, J. Waarma, and E. A. Lomonova, "Semi analytical framework for synchronous reluctance motor analysis including finite soft-magnetic material Permeability," *IEEE Trans. on Magn.*, Vol. 51, No. 11, Art. ID 8110504, 2015.
24. Djelloul, K. Z., K. Boughrara, R. Ibtiouen, and F. Dubas, "Nonlinear analytical calculation of magnetic field and torque of switched reluctance machines," *Proc. CISTEM*, Marrakech-Benguérir, Maroc, Oct. 26–28, 2016.
25. Djelloul, K. Z., K. Boughrara, F. Dubas, and R. Ibtiouen, "Nonlinear analytical prediction of magnetic field and electromagnetic performances in switched reluctance machines," *IEEE Trans. on Magn.*, 2017, DOI: 10.1100/TMAG.2017.2679686.
26. Meeker, D. C., Finite Element Method Magnetics ver. 4.2, [Online], Available: http://www.femm.info, Apr. 1, 2009.